IEEE Robotics and Automation Letters (RAL) paper presented at the
2020 IEEE International Conference on Robotics and Automation (ICRA)
31 May - 31 August, 2020. Paris, France

Shape-morphing wheel design and analysis for step climbing in high speed locomotion*

Sijun Ryu, Youngjoo Lee, TaeWon Seo, *Member, IEEE*

Abstract— **The ability of wheeled mobile robots to overcome steps is often limited by wheel size. Enhancing the ability of mobile robots to overcome obstacles is essential for extending their operation area, and many previous attempts have been made by using transformable wheels, a linkage mechanism, and a spoke-type wheel-leg mechanism. In this study, we propose a shape-morphing wheel mechanism for step climbing at high speed. In the general case of low speed locomotion, a robot's wheels can be used normally. However, to overcome relatively large obstacles, the robot's wheels can extend its shape by using the proposed morphing mechanism with centrifugal force at high speed locomotion. Two modes of step climbing are analyzed that use kinetic energy conversion or impact on the steps. Detail design issues with comprehensive analysis results are presented. Results demonstrate that a robot with morphing wheels can climb a 46.67 mm obstacle at 1.82 m/s, which is 1.33 times larger than the wheel radius. We expect that this method can be applied to other locomotion modes of wheeled mobile robots.**

Index Terms—**Transformable wheel, obstacle-overcoming, dynamic simulation, wheeled robot.**

I. Introduction

In a disaster situation, field robots need the capability to search quickly and high mobility. An example is a nuclear power plant accident. Accident area at nuclear power plant is severely radioactively contaminated and inaccessible to humans. In a radioactive contamination area, the mission of the field robot is to find the source of the accident and to locate survivors. There are many several step in the city. Not only steps but also there may be several concrete piles, debris, etc. on the ground due to the accident. In order to complete these missions successfully, the field robot needs the ability to overcome these obstacles. The ability to cross low gaps is also necessary. Therefore, in this dissertation, we focused on a novel shape-morphing wheel mechanism to meet the above conditions.

One method that can increase the obstacle-traversing abilities of wheeled mobile robots is by converting its wheels to a spoke type wheel-leg mechanism. Whegs platforms are the most popular robots that use the spoke type wheel-leg mechanism [1]. Bio-inspired tri-spokes are used to facilitate locomotion and hugely increase obstacle-traversing abilities. Loper [2] is a modified version of the tri-spoke mechanism that uses a curved spoke to climb stairs and steps more stable than the Whegs mechanism. Rising STAR [3] uses a sprawl mechanism, FBEM and wheel-legs for overcoming obstacles. IMPASS [4] also uses spokes where the lengths of spokes are changed to climb high obstacles. Spoke mechanisms are highly useful in climbing steps, but due to the discretized motion of the spokes, its agility and energy efficiency decrease on flat surfaces.

To simultaneously maintain the advantages of a wheeled mechanism and to increase its obstacle-overcoming abilities, researchers have proposed linkage-based wheeled-robots. One important design is the rocker-bogie mechanism, which is used in the Mars rover [5]. Based on the rocker-bogie mechanism, many modified mechanisms have been proposed, such as the four-bar link mechanism [6], Shrimp [7], RHyMo [8], and modified rocker-bogie with a prismatic joint [9]. These proposed mechanisms have an advantage of smooth locomotion that can overcome obstacles, while flat surface locomotion is performed by wheels. The main disadvantage of the linkage-based wheeled robots is their slow speed, because they use a static friction force to overcome steps. In addition, the mechanical complexity is very high, requiring complex control algorithms and causing failures.

Transformable wheel mechanisms have been proposed to traverse obstacles. Typically, transformable wheels operate as a wheel on a flat surface, and their shape is transformed to the spoke type when the robot meets obstacles. Due to its simple design, transformable wheels have the advantage of easy control. Yun et al. [10] developed a transformable wheel by using a pneumatic actuator with a soft structure. The robot can climb 2.9 times the robot's radius by using the spokes operated by the pneumatic actuator. WheeLeR [11] uses a reconfigurable wheel with a gear mechanism that is similar to planetary gears, thereby becoming anisotropic. The Epi. q-1 robot [12] is an important example of a transformable wheel mechanism, where the robot uses a planetary gear train to extend and shrink three small wheels attached on three spokes. Wheel Transformer [13] also uses a transformable wheel with three spokes. An important feature of the Wheel Transformer is that its transformation occurs through using external forces instead of adding an actuator. Through its minimal design sans actuator, its design and control have become simpler and efficient. Research on transformable wheels has become more popular with the recent development of soft material and smart actuators.

This study proposes a new wheel mechanism for climbing steps that are relatively larger than a wheel's radius. In low speed locomotion, a robot's wheels are used normally for horizontal movement. By designing a morphing mechanism

* This research was supported by the National Research Foundation of Korea(NRF) Grant funded by the Ministry of Science and ICT for First-Mover Program for Accelerating Disruptive Technology Development (NRF-2018M3C1B9088328(2018M3C1B9088331, 2018M3C1B9088332)).
(*Corresponding author : TaeWon Seo*)

S. Ryu, Y..Lee, and T. Seo are with the Department of Mechanical Engineering, Hanyang University, Seoul 04763, Rep. of Korea. (e-mail: fbtlwns07@hanyang.ac.kr, rp2505@hanyang.ac.kr, taewonseo@hanyang.ac.kr).

and using centrifugal force from a wheel's rotation, the wheel can change its shape to the spoke type during high speed locomotion. By using its spokes, a robot can climb relatively large steps. Via its minimal design, control of the robot is very simple. A parametric design based on a dynamic model, simulation, and experimental verification is addressed in this paper.

The rest of the paper is organized as follows. Section 2 describes the wheel mechanism and the principle of wheel transformation. Section 3 describes the dynamic model of the transformation mechanism and the parametric design based on the dynamic model. Section 4 explains the prototype design's issues with comprehensive experimental results to show the performance of the proposed wheel mechanism. Concluding remarks follow in Section 5.

II. Robot With Morphing Wheel Mechanism

A. Robot configuration

This study's robot consists of a wheel, main body, controller and battery. The main body is a rigid-body type with a tail structure that drags on the ground during locomotion. The tail has a function that transfers the reaction force to the ground to move the robot forward. The tail of the body has no wheels. When the wheels are used, the robot can be transported to the base of the stairs. A controller and battery are inside of the main body near the wheels to minimize the reaction force, and DC motors are equipped on each wheel for their operation. The mechanism configuration of the robot is shown in Fig. 1.

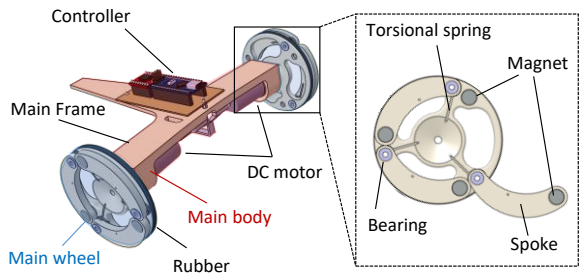

Figure 1. Shape-morphing robot configuration

The most important components of the robot are the wheels, which can change their shape based on the speed. The wheels consist of the main wheel frame and a morphing wheel. The morphing wheel is composed of three spokes that are connected by the main wheel frame. In between the main wheel frame and the spokes, a torsion spring is embedded; at the end of the spoke, magnets are embedded for holding spokes and concentrating the center of gravity to the end of the spokes.

Fig. 2 explains the wheel-morphing principle based on operation speed. At normal speed, the magnet holds the three spokes when the wheel is operated in its circular mode. When the robot meets an obstacle that the circular mode cannot overcome, the robot moves back for a "run up" to increase its speed. Through this speed increase, the centrifugal forces the magnets and the torsional spring force to open-up the three

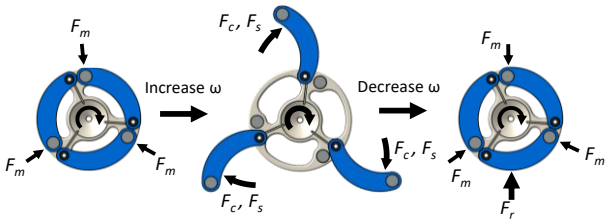

Figure 2. Explanation of the self-morphing function of the wheels according to the operation speed. F_m is the magnetic force, F_c is the centrifugal force, F_s is the spring force, and F_r is the reaction force from the ground.

spokes, which functions similarly to a large wheel. After the robot overcomes the obstacle, the spoke is folded due to the ground reaction force, and the magnetic force holds the spoke in place [12-13].

The main goal of this mechanism is to get horizontal speed and then get vertical speed, and we want to separate the act of run-up motion and impact the ground by spoke for earning vertical speed by just one actuator. To realize this run-up principle, theoretical and experimental analysis and a design parameter selection of magnets, springs, and dimensions are required.

B. Obstacle traversing scenario

The robot uses a run-up to open the spokes and uses the spokes to traverse the obstacles at high speed, as shown in the Fig. 3. To analyze the phenomena mathematically, an analysis of this scenario is required.

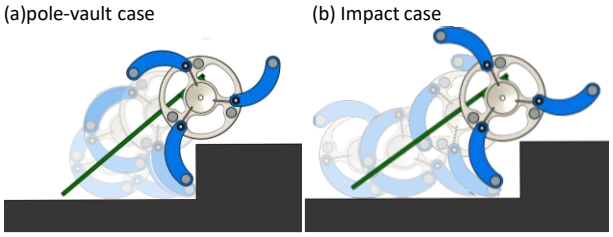

Figure 3. The scenarios of the proposed shape-morphing wheel for traversing obstacles. (a) pole-vault case, and (b) impact case.

There are two possible scenarios by which obstacles can be passed by the proposed principle of this study: (a) when the spoke hits the corner to create a pole-vault jump (pole-vault case) [14], and (b) when the spoke hits the rise of the step to generate force and make the wheel move upward (impact case). The two cases can both move a robot past an obstacle, and it is impossible to control the robot enough to make either case viable during high speed locomotion. Therefore, the analyses to consider both pole-value and impact cases are required to design the robot prototype.

III. Modeling And Simulation

A. Pole-vault case

Figure 4 shows the free-body diagram of the model for the pole-vault case. We used kinematics of the relative velocity to simulate the motion of the robot. We assumed the robot parts as a rigid body. By calculating the resulting velocity of the main body after vaulting, the ballistic model is calculated

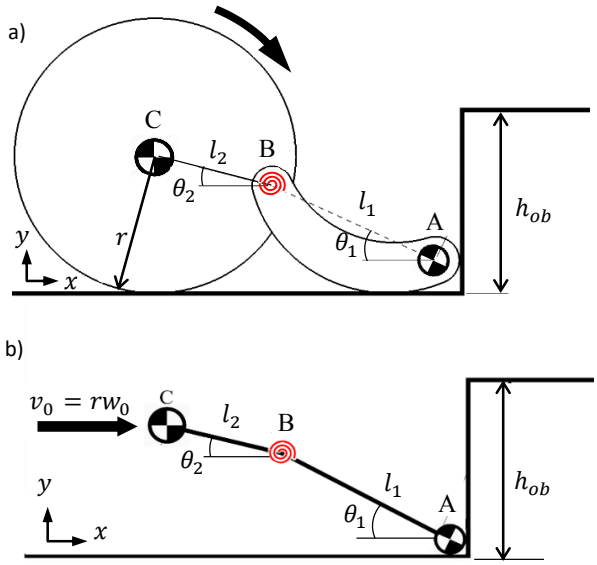

Figure 4. Free-body diagram of the robot in the pole-vault case. r is the radius of the wheel, l_1 is the length of the spoke, l_2 is the distance between the center of the main body and the revolution joint, θ_1 is the spoke angle according to the x-axis, and θ_2 is the angle of line BC according to the x-axis. (b) is a simplified model of (a). v_0 is the initial velocity of the center of wheel point C and can be expressed as $r\omega_0$. We assume that point A is fixed during angular momentum conservation.

based on an energy conservation equation. We used an assumption that the wheel and ground have no slip (which denotes $v_0 = r\omega_0$ in Fig. 4).

The velocity of the main body after vaulting can be expressed as follows:

$$\boldsymbol{v'_C} = \boldsymbol{v'_B} + \boldsymbol{v'_{C/B}}, \tag{1}$$

where v'_B is the velocity of B and $v'_{C/B}$ is the relative velocity of C with respect to B after vaulting. The initial velocity of point B is derived by the center of the wheel at point C; however, the velocity of point B after vaulting can be derived by the support fixture point A. v'_B can be calculated from the momentum conversation equations from the initial angular velocity of the wheel, ω_0, as follows:

$$\boldsymbol{v'_B} = \boldsymbol{\omega'_m} \times \boldsymbol{r_{BA}} = (l_2\omega_0 \mathrm{C}_{12} - r\omega_0 \mathrm{S}_1)[\mathrm{S}_1 \quad \mathrm{C}_1]^{\mathrm{T}}, \tag{2}$$

where ω_0 is the initial angular speed of the wheel. ω'_m is the angular velocity vector of the spoke for the bottom of step obstacle point A. C_i is the abbreviation of $cos\,\theta_i$. C_{12} is $cos(\theta_1 + \theta_2)$. S_i is $sin\,\theta_i$.

The $v'_{C/B}$ is calculated from the angular momentum conservation and kinematics as follows:

$$\boldsymbol{v'_{C/B}} = r\omega_0 \mathrm{S}_2\,[\mathrm{S}_2 \quad \mathrm{C}_2]^{\mathrm{T}}. \tag{3}$$

By substituting (2) and (3) into (1), we can obtain the final velocity of the main body. By considering only the y-directional velocity component, which is related to the jumping height, we can obtain the height based on the energy conservation equation as follows:

$$h_{pol} = \frac{(v'_C)_y^{\,2}}{2g} = \frac{1}{2g}(l_2\omega_0 \mathrm{C}_{12}\mathrm{C}_1 - r\omega_0 \mathrm{S}_1\mathrm{C}_1 + r\omega_0 \mathrm{S}_2\mathrm{C}_2)^2, \tag{4}$$

where g is the gravitational acceleration $9.8m/s^2$. h_{pol} is jumping height by pol-vault mode.

Note that θ_1 and θ_2 have geometric constraints in (5), and that the values are dependently determined from each other.

$$r = l_1\mathrm{S}_1 + l_2\mathrm{S}_2. \tag{5}$$

Therefore, there is one independent variable θ_2, regardless of the kinematic length variables, that is used to determine the final pole-vaulting height of the robot. Detailed analysis of these variables is in Fig 7. ω_0 is set to 52.16 rad/s because spokes open at that angular speed.

B. *Impact case*

A free-body diagram for the impact case is shown in Fig. 5. The model looks similar to the pole-vault model, but its calculation procedure is different. We used the dynamics of the principles of angular impulse and momentum as well as that of eccentric impact. Eventually, the main body can obtain enough velocity to jump and traverse the obstacle via the spoke's impact. We assumed that the spoke has no friction with the ground and that point B is a fixed point, because this phenomenon happened over an extremely short period of time that could not be easily measured. We then needed to derive the vertical speed at the center of wheel point C. Thus, we calculated the jumping velocity directly via the impact force and we found the restitution coefficient through a ball drop experiment for deriving the impact force.

The basic equation of the impact case is as follows:

$$+\circlearrowleft)\ I_m\omega_m + \int d_{im}\,P\,dt = I_m\omega'_m. \tag{6}$$

$$+\uparrow)\ Mv_{M_y} + \int P\,dt = Mv'_{M_y}. \tag{7}$$

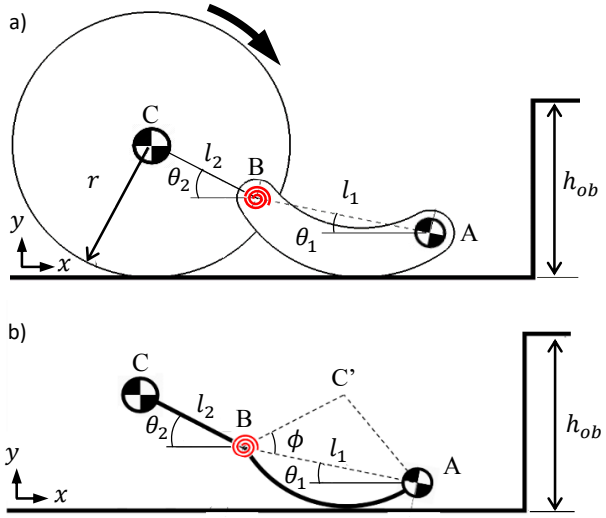

Figure 5. Free-body diagram of the robot in the impact case. r is the radius of the wheel, l_1 is the length of revolution joint B and the spoke's center of mass point A, l_2 is the distance between the center of the main wheel and joint B, θ_1 is the spoke angle according to the x-axis, and θ_2 is the angle of line BC according to the x-axis; ϕ is the angle of between BC' and l_1, this value is constant. Note that C and C' have the same height above ground during spoke impact, and joint B has a torsion spring. (b) is a simplified model of (a). we can define $\theta_1 + \theta_2 = \angle ABC'$ (= 38.7 deg) when the spoke contacts the ground through the geometrical shape of the wheel.

where I_m is the inertia of the spoke at point B. $\int P\,dt$ is the impact force that has d_{im} horizontal distance at joint B. when the ground is flat, the impact force always operates vertical side. ω_m is the angular velocity before the spoke impact, where we have an assumed fixed point at B. ω'_m is the spoke's angular velocity after impact of a spoke. m is the spoke's mass, while M is the sum of the wheel mass and half of the main body. v_{m_y} is the vertical velocity at the center of the spoke mass before impact. v'_{m_y} is after the spoke impact.

From (6), the impact force can be calculated as follows:

$$\int P\,dt = \frac{I_m}{d_{im}}(\omega'_m - \omega_m) = -\frac{I_m}{d_{im} l_1}(e+1)v_{m_y}\mathrm{C}_1, \quad (8)$$

where e is 0.78 and this value is determined by the experiment. d_{im} is l_2C_2 as shown in Fig. 6.

As shown in (8), to calculate the impact force the spoke speed must be determined before contact with the ground, and the wheel-spoke system can be expressed by a two-linked pendulum. A dynamic equation can be derived by the Lagrangian method, and we assume that the gravitational force is zero as follows:

$$\mathbf{J}\begin{pmatrix}\ddot{\theta}_1\\ \ddot{\theta}_2\end{pmatrix} + q_{\mathrm{C}}\begin{pmatrix}\ddot{\theta}_2\\ \ddot{\theta}_1\end{pmatrix} + q_{\mathrm{S}}\mathbf{q}_{\mathbf{I}}\begin{pmatrix}\dot{\theta}_2\\ \dot{\theta}_1\end{pmatrix}^{\mathrm{T}}\begin{pmatrix}\dot{\theta}_2\\ \dot{\theta}_1\end{pmatrix} + k(\theta_1 - \theta_2 + \varepsilon)\mathbf{q}_{\mathbf{I}} = \begin{pmatrix}\tau\\ 0\end{pmatrix}. \quad (9)$$

TABLE I. VARIABLES FOR DYNAMIC EQUATION 9

Symbol	*Variable*
J	$\begin{pmatrix} I_M + ml_1^2 & 0 \\ 0 & I_m + ml_2^2 \end{pmatrix}$
$\mathrm{q_I}$	$\begin{pmatrix} 1 & 0 \\ 0 & -1 \end{pmatrix}$
q_{C}	$ml_1 l_2 \cos(\theta_1 - \theta_2)$
q_{S}	$ml_1 l_2 \sin(\theta_1 - \theta_2)$

I_M is the inertia of the wheel at point C. k is a spring constant. ε is the offset of the spring at a closed spring $\pi/4$ in radian. The vertical speed of the spoke can be expressed as follows:

$$v_{m_y} = l_1\dot{\theta}_1\mathrm{C}_1 + l_2\dot{\theta}_2\mathrm{C}_2. \quad (10)$$

The reaction force can be calculated by equation (8). At this moment, only one unknown is present, and $\int P\,dt$ solves the vertical velocities of the main body and wheel. $\dot{\theta}_1$ and $\dot{\theta}_2$ are defined by the assumption that the gravitational force is zero, with a constant initial angular velocity of the wheel and constant torque. Both angles also constrain each other when contacting the spoke at the ground as shown in Fig. 6.

$\int P\,dt$ is a function of $\theta_1, \theta_2, v_{m_y}$. If the input torque is constant, these factors can be defined by θ_1 when the spoke contacts the ground. The θ_1 region ranges from 90° to 0° via the wheel's form. The last step of calculating the vertical velocity of the body is obtained in (7). v_{M_y} is zero because there is no factor for the vertical acceleration before impact. v'_{M_y} occurs after impact and $\int P\,dt$ is obtained at (8).

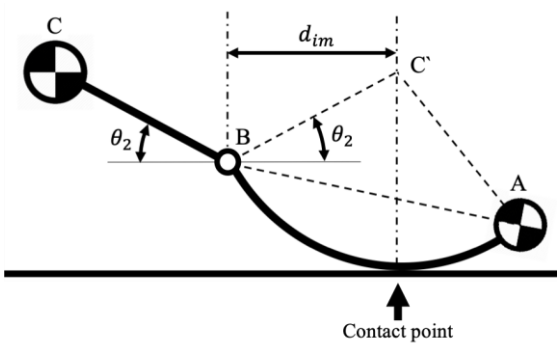

Figure 6. Free-body diagram of the spoke in the impact case. d_{im} is the horizontal distance between the contact point and joint B, and it can be derived by the geometrical shape. The impact force acts on the spoke at the contact point. Note that line BC and line BC' have the same length as l_2.

Based on the energy conversion equation in ballistic motion, we can obtain the height as follows:

$$h_{imp} = \frac{{v'_{M_y}}^2}{2g} = \frac{1}{2g}\left[\frac{1}{M}\frac{I_m}{l_1 l_2}(e+1)v_{m_y}\frac{\mathrm{C}_1}{\mathrm{C}_2}\right]^2. \quad (11)$$

where h_{imp} is jumping height by impact mode. We acquired the jumping height when the spoke hit the ground once. The graph of equation (11) is shown in Fig. 7.

C. Sensitivity analysis on the design parameters

Based on the model in previous sections, we attempted to determine the design parameters for the robot prototype. The wheel radius, body mass, and wheel mass are fixed based on the prototype design, and we varied the spoke mass, spoke length, and the distance between the wheel center to the spoke for use in the sensitivity analysis.

Figure 7 shows the sensitivity results of the design parameters to the obstacle-height when the initial contact angle (θ_2) is changed. The pole-vault and impact cases have different results. In the pole-vault case, θ_2 is very dominant within the vertical speeds of the wheel and the robot body. According to (2) and (3), equation (2)'s unit spans three decimal places and is almost zero, which means that the velocity of the spoke is close to zero during the vaulting phase. Thus, the velocity of the spoke has a small effect; namely, the angle of the wheel is dominant on jumping at equation (2). Therefore, in Fig. 11(g), the morphology of the spoke can be observed between dynamic movements. Based on the result of the sensitivity analysis, we designed the robotic prototype and performed our experiments as explained in Section IV.

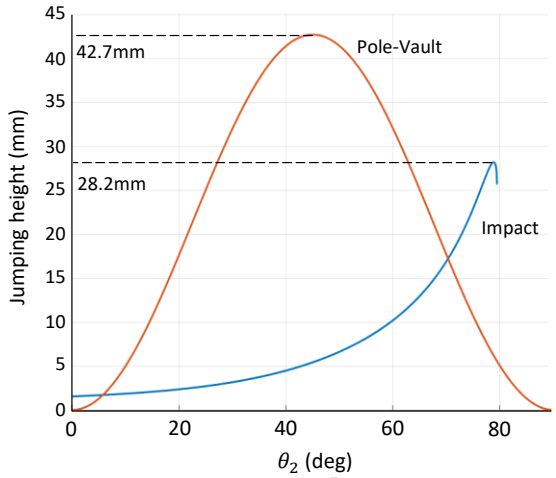

Figure 7. Sensitivity analysis of the pole-vault case and impact case. The pole-vault mode saw the robot jump higher than in impact mode, but the wheel had three spokes. The spokes hit the ground periodically. The robot gained potential energy by hitting the ground. The maximum point during the pole-vault jump was 42.7 mm at 45 degrees and at the impact it was 28.2 mm at 78.92 degrees. Initial angular velocity of spoke at impact case can be derived by θ_2 and the initial angular velocity of the wheel at pole-vault is 52.16 rad/s. This angular speed was derived by experimental data at spoke opening speed.

IV. Prototype And Experiments

A. Prototype and Specification

Fig. 8 shows the robot prototype with the shape-morphing wheels. The size of the prototype is 212×190×70 mm^3 and the weight is 0.291 kg, including the battery. We used Arduino (Nano) as a controller for both the wheel speed control and the Lithium-polymer battery cell (HAN, 3.7 V 1.85 Wh). To decrease the mass, we chose an extremely small polymer battery, and to obtain high voltage we connected it to a series of three cells. Two geared DC motors (D&J with, DC 6 V Max. 3 kg-cm) are used to rotate the wheels with an embedded encoder. We selected the motors with an encoder to control both the motor's phase and to improve the straightness of the robot. Three magnets for each wheel were embedded (Neodymium). At the edge of the wheels, we used rubber to avoid slippage between the ground and wheels. The selected design parameters in Section 3 were used to manufacture the parts, and most of the manufactured parts were made using a 3D printer (F123 series, Stratasys).

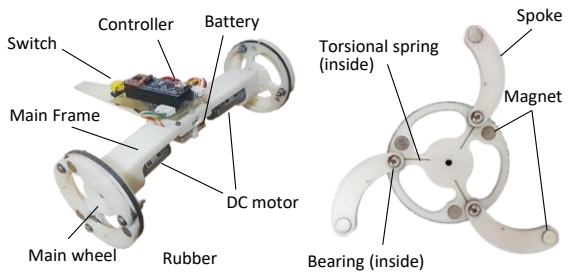

Figure 8. Self-morphing robot prototype for obstacle-overcoming in high speed.

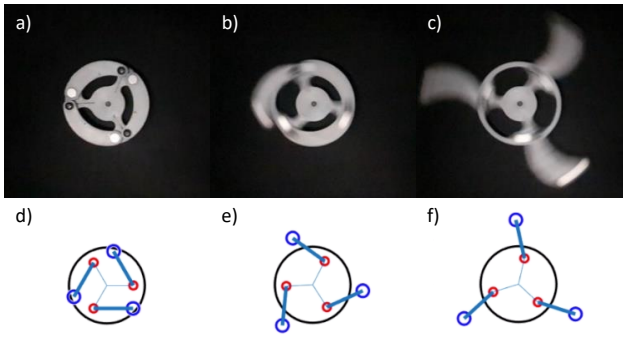

Figure 9. Spoke-open in high speed rotation. a)-c) are spoke-open is real. d)-f) are simulated figure. by a),d) zero-speed, b),e) Spoke spread-speed ($\omega_{spread} = 52.16\, rad/s$), and c),f) high-speed.

The self-morphing wheel of the robot prototype is shown in Fig. 9. As the speed increased, the centrifugal force increased over the magnetic attachment, and the spoke opened. Note that the spoke did not fold since there was no ground reaction force to retrieve the spoke, but the spoke could fold during ground rotation due to the robot's weight. The robot changed the wheel mode through only its wheel velocity.

B. Experimental setup

We focused on observing the ability of the shape-morphing wheel. The robot had no sensor without the encoder in the motor. The snapshot of Fig. 9 was captured by a high-speed camera. To obtain straightness, we designed a toe-in angle of approximately 5 degree. Theoretically, a wheel cannot overcome an obstacle that is higher than its radius. Therefore, we set the height of the obstacle to 1.33 times higher than the radius. To prevent a reverse current that occurred when the spoke hits the bottom, the bypass circuit was configured separately. The simulation and experimental results are presented in the Multimedia extension.

C. Experimental results

Figure 10 shows the experimental results of the developed robot prototype. We used an obstacle at 46.67 mm in height, which is 1.33 times longer than the wheel radius. The speed of the robot is 1.82 m/s. As seen in the Fig. 10(a-d), the robot could not overcome the obstacle with a static wheel. However, by using the shape-morphing wheel, the robot overcame the obstacle. In both the pole-vault and impact cases, Fig. 10(e-i) and Fig. 10(j-m), respectively, the robot overcame the obstacle, and then the wheel was easily changed back to its normal circular mode. The detail experimental results are presented in the Multimedia extension.

Notably, the robot overcame obstacles without adding any actuators. The robot was actuated by the wheel motors as usual and the robot overcomes the obstacle at high-speed by using kinetic energy instead of potential energy as presented in [17]. We attempted to align the robot with the obstacle for the experiment, as alignment was an important requirement. Through the use of the morphing wheel mechanism, we expect that the operating spaces of robots will be widened in various applications.

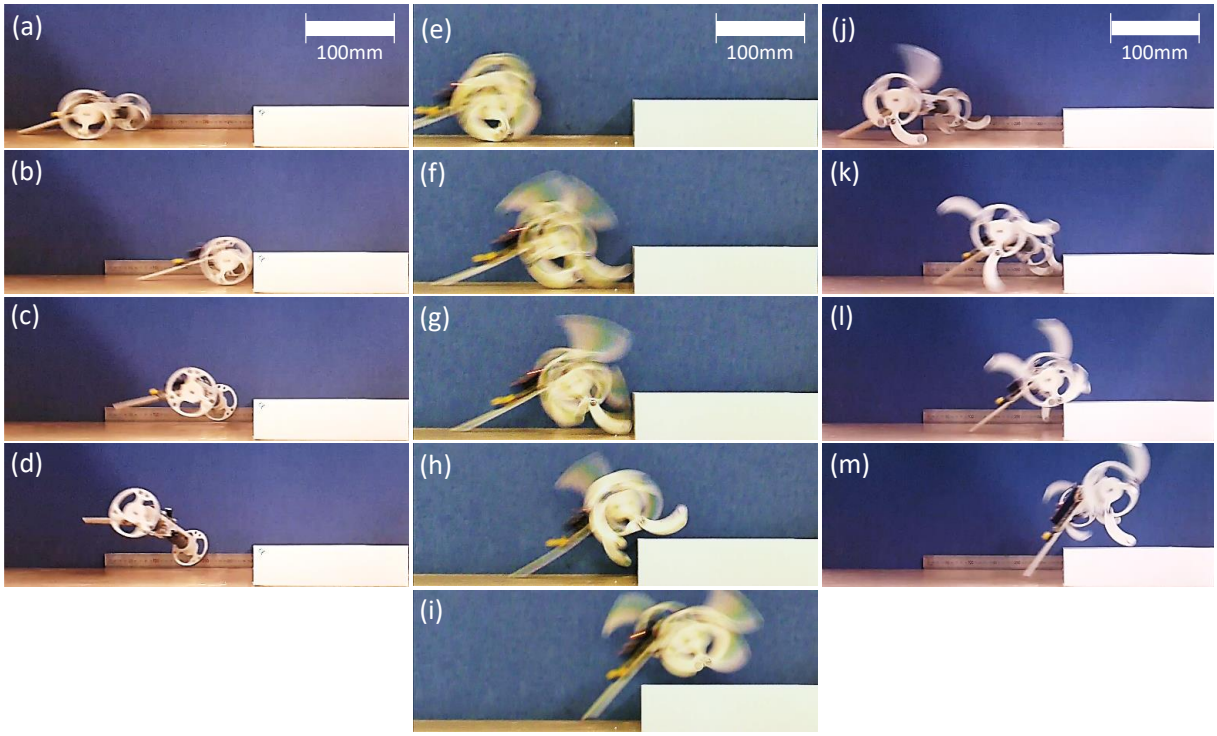

Figure 10. Snapshots during obstacle-traversing, (a)-(d) with static wheels, (e)-(i) pole-vault case, and (j)-(m) impact case (see Multimedia extension).

V. Conclusion

This study proposed a shape-morphing mechanism for a wheeled robot to overcome a relatively large obstacle. The robot is composed of a main body and two shape-morphing wheels. The shape morphing wheels consist of a rigid circular wheel with three spokes with a magnetic attachment. At a low speed, the spoke is closed to create a circular wheel, and at a high speed, the centrifugal force operating on the magnets opens the spoke to be used in traversing obstacles. Two possible scenarios for pole- vault and impact cases and the sensitivity on the design parameters were analyzed. This experiment proved that our robot prototype can overcome an obstacle of 1.33 times its wheels' radii, which is normally not possible with static wheels. We expect that this wheel mechanism will ultimately be used in search and rescue missions in unstructured environments.

References

[1] A. S. Boxerbaum, J. Oro, G. Peterson, R. D. Quinn, "The latest generation of WhegsTM robot features a passive-compliant body joint," IEEE/RSJ International Conference on Intelligent Robots and Systems, Nice, France, 2008.

[2] S. D. Herbert, A. Drenner, N. Papanikolopoulos, "Loper: a quadruped-hybrid stair climbing robot," IEEE International Conference on Robotics and Automation, Pasadena, CA, USA, 2008.

[3] D. Zarrouk, L. Yehezkel, "Rising STAR, a highly reconfigurable sprawl tuned robot," IEEE International Conference on Robotics and Automation, Brisbane, Australia, 2018

[4] J. B. Jeans, D. Hong, "IMPASS: intelligent mobility platform with active spoke system," IEEE International Conference on Robotics and Automation, Kobe, Japan, 2009.

[5] H. S. Hong, T. Seo, D. Kim, S. Kim, J. Kim, "Optimal design of hand-carrying rocker-bogie mechanism for stair climbing," Journal of Mechanical Science and Technology, vol. 27, no. 1, pp. 125-132, 2013.

[6] H. D. Choi, C. K. Woo, S. Kim, W. K. Kwak, S. Yoon, "Independent traction control for uneven terrain using stick-slip phenomenon application to a stair climbing robot," Autonomous Robots, vol. 23, no. 1, pp. 3-18, 2007.

[7] T. Estier, Y. Crausaz, B. Merminod, M. Lauria, R. Piguet, R. Siegwart, "An innovative space rover with extended climbing abilities," Proceedings of Space and Robotics, Albuquerque, USA, 2000.

[8] D. Choi, Y. Kim, S. Jung, J. Kim, H. S. Kim, "A new mobile platform (RHyMo) for smooth movement on rugged terrain," IEEE/ASME Transaction on Mechatronics, vol. 21, no. 3, pp. 1303-1314, 2016.

[9] H. Hong, Y. Jeon, J. Kim, H. S. Kim, "Development of a new hybrid link based mobile platform," International Conference on Control, Automation and Systems, Busan, Korea, 2015.

[10] S.-S. Yun, J.-Y. Lee, G.-P. Jung, K.-J. Cho, "Development of a transformable wheel actuated by soft pneumatic actuators," International Journal of Control, Automation and Systems, vol. 15, pp. 1-9, 2016.

[11] C. Zheng, K. Lee, "WheeLeR: Wheel-leg reconfigurable mechanism with passive gears for mobile robot applications," International Conference on Robotics and Automation, Montreal, Canada, May 20-24, 2019.

[12] G. Quaglia, D. Maffiodo, W. Franco, S. Appendino, R. Oderio, "The Epi.q-1 hybrid mobile robot," International Journal of Robotics Research, vol. 28, no. 1, pp. 81-91, 2010.

[13] Y. Yamada, G. Endo, T. Nakamura, "Blade-type crawler vehicle with wings in ground effect for traversing uneven terrain at high speed," IEEE/RSJ International Conference on Intelligent Robots and Systems, Daejeon, Korea, 2016.

[14] Y.-S. Kim, G.-P. Jung, H. Kim, K.-J. Cho, C.-N. Chu, "Wheel Transformer: a miniaturized terrain adaptive robot with passively transformed wheels," IEEE International Conference on Robotics and Automation, Karlsruhe, Germany, 2013.

[15] J. Choi, K. Jeong, T. Seo, "Pol-E: Large-obstacle overcoming by energy conversion method using an elastic link," International Journal of Control, Automation, and Systems, vol. 15, no. 4, pp. 1835-1843, 2017.

[16] K. Misu, A. Yoshii, H. Mochiyama, "A compact wheeled robot that can jump while rolling," IEEE/RSJ International Conference on Intelligent Robots and Systems, Madrid, Spain, 2018.

[17] Y. Yamada, T. Nakamura, "Blade-type crawler capable of running on the surface of water as bio-inspired by a basilisk lizard," IEEE/RSJ International Conference on Intelligent Robots and Systems, Madrid, Spain, 2018.